Temperature Dependence of Qubit Decoherence and Applications for Optimizing Quantum Hardware

Edward Wu
Pittsford Sutherland High School
Pittsford, NY, USA

Mentor: **Ray Parker**
University of Rochester
Rochester, NY, USA

Temperature Dependence of Qubit Decoherence and Applications for Optimizing Quantum Hardware

Edward Wu

September 5, 2022

Abstract

Decoherence is the loss of a qubit's ability to maintain its superposition and thus capacity to perform quantum computations in the face of environmental noise. Since the invention of the transmon qubit in 2007, understanding the fundamental limits of qubit coherence has been an active field of research because their short coherence times are the greatest obstacle preventing a collection of qubits from being turned into a practical quantum computer. At higher temperatures, these decoherence times diminish. Understanding this thermal limit thus provides insight into the noise that prevents productive qubit operation overall. Theory and analytical models of the temperature dependence have been established for longitudinal relaxation time (T_1), pure dephasing (T_ϕ), and thus transverse relaxation, (T_2), which is a combination of both. This research studies these models and their mechanisms and explores the combination of a T_1 and T_ϕ model that describes T_2 dependence with temperature. In addition, it is found that as the temperature is raised the decoherence times of independent qubits begin to converge onto one value and the underlying mechanism is investigated and explained. Finally, this research proposes an optimization application based on this converging phenomenon by thermally inducing a decoherence-identical chip for better gate fidelity measurements.

Keywords: Superconducting qubits, transmon, T_1, T_2, T_ϕ, decoherence, temperature-dependence

Contents

1 Introduction

1.1 Background

Quantum computing is widely believed to be the next big progression in computers, giving us immense computational power to solve "unsolvable" problems like large integer factorization, in a matter of seconds. While a classical bit can assume only one of two states, 0 or 1, a qubit can assume 0, 1, or a superposition of both [13]. This effectively means that a single qubit can take on two classical values at once, two qubits can take on four classical values at once, and n qubits can take on 2^n values at once. Theoretically, a quantum computer with 300 qubits could store and process $2^{300} = 2.04 \times 10^{90}$ bits of information which is more than the number of atoms in the visible universe, around 10^{80} [6]. As a result, harnessing the computational potential of quantum systems is one of the most active fields of study in physics today. The superconducting qubit is a leading qubit type in quantum computing used in both IBM's and Google's quantum computers [4, 18] and has even been shown to achieve quantum advantage, the goal of producing a quantum computer that can solve a problem no classical computer can solve [2].

Superconducting qubits store their information in microfabricated superconducting electronic circuit elements that behave quantum mechanically at low temperatures (below critical temperature, T_c) [7]. To maintain such a low operation temperature, He-3 dilution fridges are needed, which represents one of the superconducting qubit's biggest limitations: they must be cooled to millikelvin temperature scales to become quantum systems. However, its great advantage lies in the fact that many superconducting qubits can be fabricated on a single chip like classical CPUs. As a result, superconducting qubits are compatible with already existing nanofabrication infrastructure [17].

The transmon, a type of superconducting qubit, was developed in 2007 with the goal of overcoming the second main challenge of turning a collection of qubits into a quantum computer: short dephasing times [8]. In quantum mechanics, coherence refers to the ability of a qubit to maintain a superposition state and thus its ability to perform quantum computations in face of environmental noise and the effects of thermalization [9]. Decoherence is the loss of quantum coherence caused by environmental noise. The transmon's design is based on the charge qubit (Cooper-pair box), a superconducting circuit island that consists of a capacitor coupled to a Josephson junction. The state of the qubit is determined by the number of Cooper pairs that tunnel through the Josephson junction [12]. The transmon was designed to significantly improve dephasing times caused by charge noise.

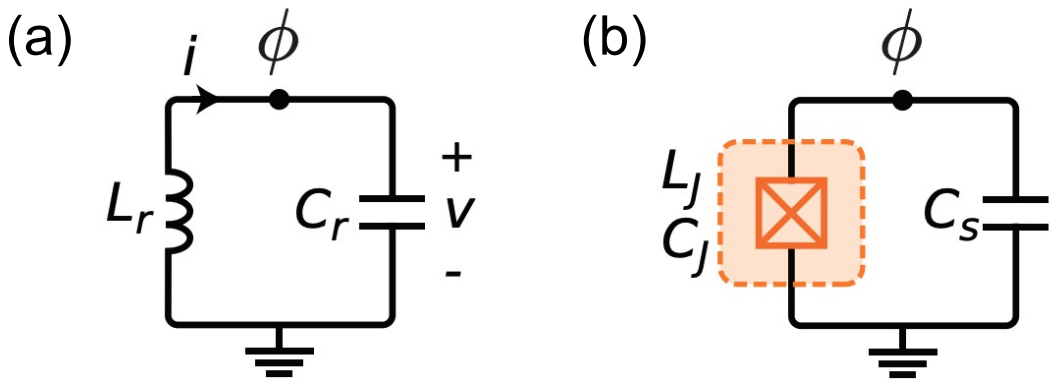

Figure 1: Transmon Circuit Diagram. (a) Depiction of an LC (Inductor-Capcitor) circuit which acts as a harmonic oscillator. (b) Diagram of a charge qubit which consist of a Josephson junction (orange) and capacitor (C_s) and acts as a quantized version of the LC circuit. Because of the Josephson junction, a charge qubit has discrete energy levels which is why it is sometimes referred to as an "artificial atom." Figure source: [10].

There are three main decoherence times: longitudinal relaxation (T_1), pure dephasing (T_ϕ), and transverse relaxation (T_2) [10]. This research focuses on understanding the temperature dependence

of these three forms of decoherence as well as an interesting converging phenomenon that can be used in applications for improving qubit performance measurements.

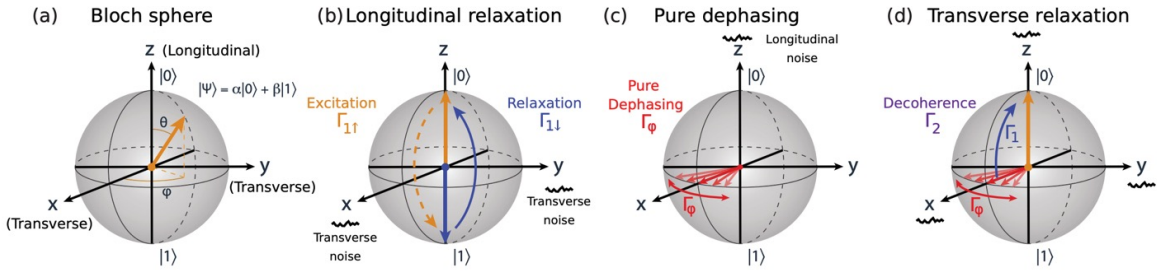

Figure 2: Decoherence shown on the Bloch sphere. (a) The Bloch sphere is a 3-D unit sphere used commonly to represent a qubit [1]. The north pole represents a ground state $|0\rangle$ and the south pole represents the first excited state $|1\rangle$. All other vectors that touch the surface area of the sphere (magnitude = 1) represent a pure quantum state, meaning the qubit is in superposition. Vectors not touching the surface of the sphere (magnitude $\neq 1$) represent a mixed state. (b) Longitudinal relaxation represented as a summation of up rate and down rate. In cryogenic temperatures, the excitation rate is generally non-existant. (c) Pure dephasing shown as the spreading of a vector along the equator of the sphere. (d) Transverse relaxation as a combination of longitudinal rate and pure dephasing rate. Figure source: [10].

1.1.1 Longitudinal Relaxation (T_1)

The longitudinal relaxation time, T_1, is the characteristic time scale for a qubit in cryogenic conditions to naturally "relax" from $|1\rangle$ to $|0\rangle$ after excitation due to losing energy to its environment. T_1 can also be represented as a rate [10],

$$\Gamma_1 \equiv \frac{1}{T_1}.$$

It is best envisioned in the Bloch sphere as the process where the qubit relaxes from the south pole to the north pole of the sphere (vertically). Longitudinal relaxation directly limits the time that a qubit stays in a desired state to perform quantum computations. A qubit with $T_1 = 60$ μs means that it goes from the $|1\rangle$ state to $|0\rangle$ on the order of 60 μs. More importantly, though, is that this 60 μs is all the time that can be used to perform computations because once the qubit is no longer in superposition, we lose all its encoded information. Currently, quantum operations take on the order of 10's of nanoseconds [3]. At best this amounts to around 3000 computations which is not enough to perform useful operations and solve interesting problems [19]. In short, current gate times and decoherence times limit the scale of quantum computations we can perform.

1.1.2 Pure Dephasing (T_ϕ)

Pure dephasing, T_ϕ, is caused by noise that fluctuates qubit frequency, which adds random fluctuations to the qubit's phase (represented as the azimuthal angle on the Bloch sphere) at a rate Γ_ϕ. This can be imagined as preparing the state vector of a qubit on the equator of the Bloch sphere (superposition), the pure dephasing time is the is the time scale over which the vector spreads across the Bloch sphere equator (horizontally). As a rate it can be represented as [10],

$$\Gamma_\phi \equiv \frac{1}{T_\phi}.$$

A pure dephasing time provides a time scale in which the quantum information can be retained. A $T_\phi = 50$ μs means that after pulsing the qubit to a superposition state, 50 μs is all we have before the qubit loses its "quantumness" and becomes indistinguishable from a classical randomly prepared bit.

1.1.3 Transverse Relaxation (T_2)

Transverse Relaxation (dephasing time), T_2, is a combination of energy relaxation and pure dephasing. In rate form, Γ_2, it can be mathematically given as [10],

$$\Gamma_2 \equiv \frac{1}{T_2} = \frac{\Gamma_1}{2} + \Gamma_\varphi.$$

Because of this relationship, given two decoherence times, it is possible to find the third decoherence time. In the Bloch sphere, transverse relaxation can be visualized by starting with the state vector on the equator of the sphere (after a $\pi/2$ pulse about the z-axis) and observing the pure dephasing behavior of the vector spreading across horizontally while simultaneously exhibiting longitudinal relaxation back to $|0\rangle$. All of these components of qubit decoherence present a fundamental limit in turning the qubit system into a practical quantum computer.

1.2 Previous Work

The paper detailing the invention of the transmon goes over seven sources of noise affecting T_1 including spontaneous emission, the Purcell Effect, dielectric loss, and flux coupling [8]. However, only one of these sources, quasiparticle tunneling, varies with temperature. They note that the population of quasiparticles will increase as temperature is raised and provide an equation expressing the relationship between the temperature and the number of quasiparticles. Furthermore, it was concluded that quasiparticles should not contribute significantly below temperatures of ∼100 mK noting that in typical dilution refrigerator conditions below 20 mK, quasiparticle noise does not limit T_1. Above temperatures greater than 100 mK, however, T_1 was predicted to begin decreasing in a non-linear relationship due to quasiparticle tunneling noise [8].

A thesis by Sears further explored the T_1 dependence with temperature using a 3D transmon of an Al-AlO-Al junction with Al electrodes. They agree that "the decrease in T_1 comes from the thermal activation of quasiparticles in the junction which damp the qubit mode" [16]. Furthermore, they provide a mathematical model describing the inverse quality factor of the qubits which can be used as a model for T_1. The same paper provides a theory for T_ϕ, based on the number of thermally induced photons in a readout resonator which shifts the transition frequency of the qubit and dephases the qubit. Their generalization model of the dephasing rate of a qubit is connected to temperature by mean photon population, n, which is dependent on the thermal bath population. However, the observation of converging decoherence times as temperature increases is not discussed in either of the prior papers which my research addresses and applies.

2 Methodology

2.1 Chip Setup

The chip that was used in this research was a 6-transmon qubit chip designed and fabricated by MIT Lincoln Laboratory nicknamed "Candle." The "Candle" was synthesized by depositing thin film superconducting Aluminum on silicon wafers via lithography and etching. The device was designed to be operated in the microwave frequency spectrum. Each qubit acts independently of the others and are all able to be excited at a slightly different microwave frequency. Each qubit also has a readout resonator coupled to it. When a qubit changes from a ground state to an excited state, the frequency of the resonator will shift, which can be detected as a change in the phase of a wave that is bounced off the resonator. The Candle has no individual drive lines (as seen in Figure 3) and was specifically designed to have high T_1 and T_2 times.

To cool the chip, a dilution refrigerator is used which can cool the sample down to 9 mK. The refrigerator contains a simple resistor as a means to heat up the system and raise the temperature. A Vector Network Analyzer (VNA) is used to locate resonator frequencies. To control and read out the qubits, several instruments are used to control input and output microwave frequencies which make up the microwave setup. First, an arbitrary waveform generator (AWG) is used to create various waveform shapes in any sequence and at any voltage. However, the AWG cannot exceed a frequency of 1 GHz. To reach higher frequencies, a local oscillator (LO) is used which generates a constant tone closer to the qubit frequencies (between 3 and 4 GHz). Thus, these two instrument outputs are

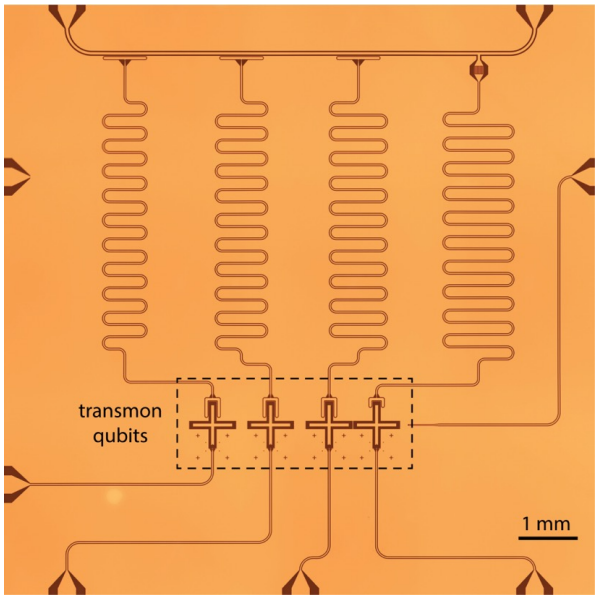

Figure 3: Chip design of a 4-transmon qubit chip. The Josephson junction is located within the cross and the snake-like wire represents the circuit. The remaining straight lines are drive or readout photon lines. Note that this figure is not the "Candle" in which we performed all measurements but a chip with similar design. Image source: [15].

combined via IQ modulation to create a desired pulse with the right shape and high enough frequency. Next, a beam combiner is used to combine the drive and readout signals and send them to the chip. Lastly, the readout signal is sent to an Analog to Digital Converter (ADC) which gets a signal from the fridge and translates to a digital signal which is processed by a computer for readout and control of the microwave setup.

2.2 Measurements

Several scans were used in extracting the T constants at each temperature. A Rabi scan measures the time for a pulse of microwave radiation at the qubit's resonant frequency to excite the qubit from its ground state to its excited state. It is used to calibrate the pulse amplitude to get a π pulse in 30 ns. The scan involves sending microwave radiation to the qubit at its resonant frequency, which continuously rotates it from its ground state to the excited state and back to ground. We measure the qubit at different points in time along the oscillation to find the Rabi oscillation rate. At each point along in time, the scan reads out from 1000 to 8000 singular measurements of either $|1\rangle$ or $|0\rangle$ with associated classical and quantum noise. From this information, we take an average of $|1\rangle$ measurements over total measurements to represent a probability of measuring the qubit in the $|1\rangle$ state.

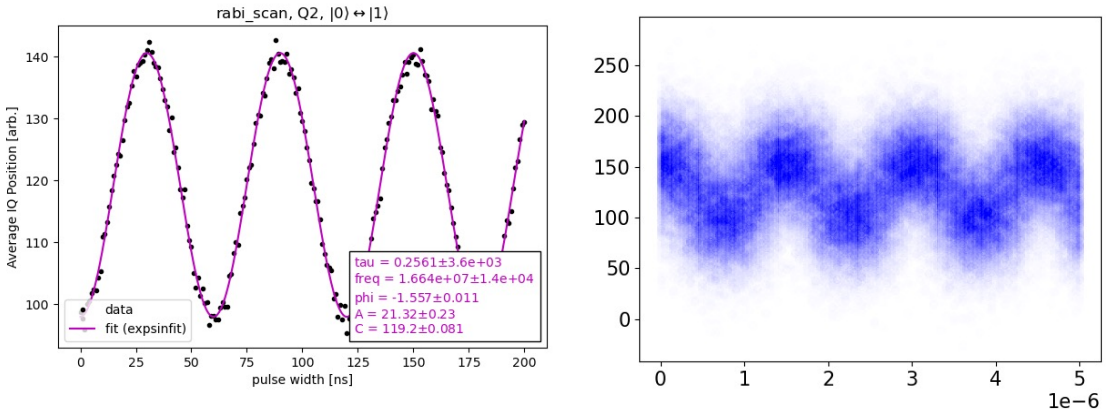

Figure 4: Rabi scan plots. (a) Measurement of a Rabi oscillation over time with averaging on. The x-axis represents time, and the y-axis represents the qubit state. Each point represents an average of several $|0\rangle$, $|1\rangle$ measurements per point in time. The purple curve represents a model fit to the points from which values can be extracted. (b) A "quantized" version of a Rabi oscillation with averaging off. Each blue point represents a single measurement of $|0\rangle$ or $|1\rangle$ per point in time.

The Ramsey scan is a common way to measure the detuning frequency of a qubit, which is defined as the difference between the frequency used for the control of rotation pulses and the actual frequency of the qubit. To perform the measurement, we prepare the qubit to a superposition state with a $\pi/2$ pulse, wait for some time t, then apply a second pulse and read out [14]. During the time that we idle between the first and second $\pi/2$ pulse, the qubit's frequency will drift induced by the detuning between the drive and the qubit. As a result, the plot of measuring probability of the excited state over time should follow a sinusoidal curve, from which we can extract f, the detuning frequency.

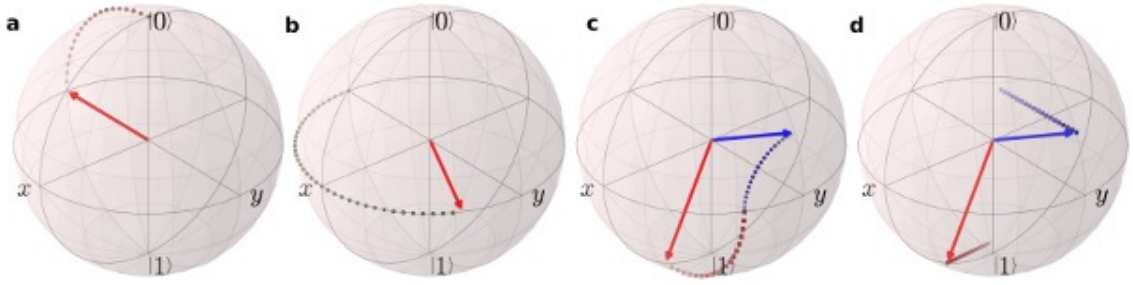

Figure 5: Bloch sphere representation of a Ramsey procedure. (a) Bloch vector after a $\pi/2$ pulse from ground state. (b) During the time that we idle, t, the vector spreads across the equator of the sphere. (c) Another $\pi/2$ pulse is performed for readout. The blue and red vector positions represent two variations of a $\pi/2$ pulse. (d) Lastly, readout is performed by measuring a probability of the qubit being in the excited state. Figure source: [14].

To extract T_1 we perform a measurement of the excited qubit after a delay. Due to decoherence processes, after some delay, the qubit may no longer be excited anymore. A T_1 scan works by fixing a delay time t and a number of shots s, in which we only excite the qubit once per shot s. By repeating the procedure of exciting a qubit s times, waiting time t, then measuring the qubit state, the probability of being in the excited state, or P(1), can be estimated. We then repeat this process for a range of delay times t to get a set of probability estimates. The resulting P(1) vs Delay (μs) should follow an exponential curve, from which we can extract the value of T_1 [19].

To extract T_2 we perform an Echo measurement. The Echo sequence is a slightly modified Ramsey measurement. After following the Ramsey procedure and reaching the idle step for time t, the Echo

enacts a π pulse to counteract the effect of offsets to the qubit frequency [14]. In the Bloch vector, as each of the vectors spreads across the equator at a different rate, a π pulse will reverse this process and allow the vectors to reconverge onto one. This state is then pulsed backed down with a final $\pi/2$ pulse. However, this process sees the decay in amplitude over time of the vector. To extract a value for T_2, the P(1) vs Delay (μs) again should assume an exponential decay model in which T_2 can be extracted [19].

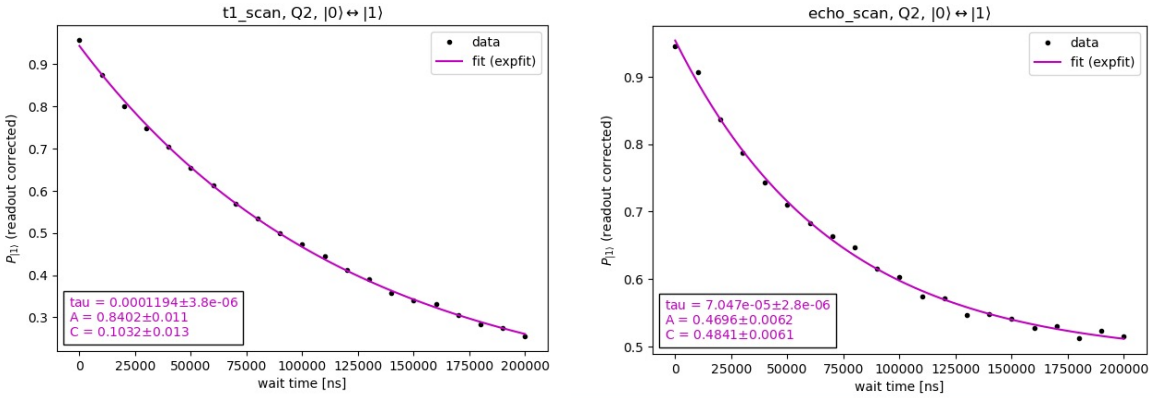

Figure 6: T_1 and T_2 plots from which we can extract decoherence times. (a) The data points in the T_1 scan plot decays in an exponential relationship with time. The purple curve represents a model fit, from which tau or T_1 can be extracted (b) A T_2 scan done by an Echo measurement yields a similar plot and curve fit from which T_2 can be extracted.

2.3 Procedure

We start by locating the resonance frequency of all 6 coupled readout resonators using the VNA. Each resonance frequency can be plotted as a function of frequency with magnitude or phase. Next, we locate the qubit transition frequency, ω_q, by continuously monitoring the state of the qubit with the readout resonator. By sending in microwave radiation at different frequencies around the range we expect to find the qubit's transition frequency, we eventually reach ω_q. We locate ω_q for the three qubits denoted Q2, Q3, and Q4 on the "Candle" chip. A Rabi scan is used to calibrate the length of pulses. Next, we use a Ramsey to measure detuning frequency to determine if the qubit frequency has shifted and needs to be redefined. When all calibrations and checks are accurate, a T_1 scan is used to extract T_1 and an Echo scan to extract T_2. This process is repeated for all three qubits before raising the temperature in the fridge to collect another data point.

3 Results

3.1 Data

The T_1 data showed three important trends. First, the data is quite noisy. However, this is to be expected because it is known that T_1 fluctuates in a random fashion with time even at the coldest temperature we can reach with the fridge (Fig. 8). Second, T_1 seems to be maintained until a threshold temperature around 120 mK after which it decreases. Third, despite measuring three independent qubits with different frequencies, above $\sim$120 mK the data points converged onto one line trend line showing less and less random variation. This collapsing tells us that above a certain cutoff temperature the temperature-induced noise will begin to overpower all other sources of qubit noise.

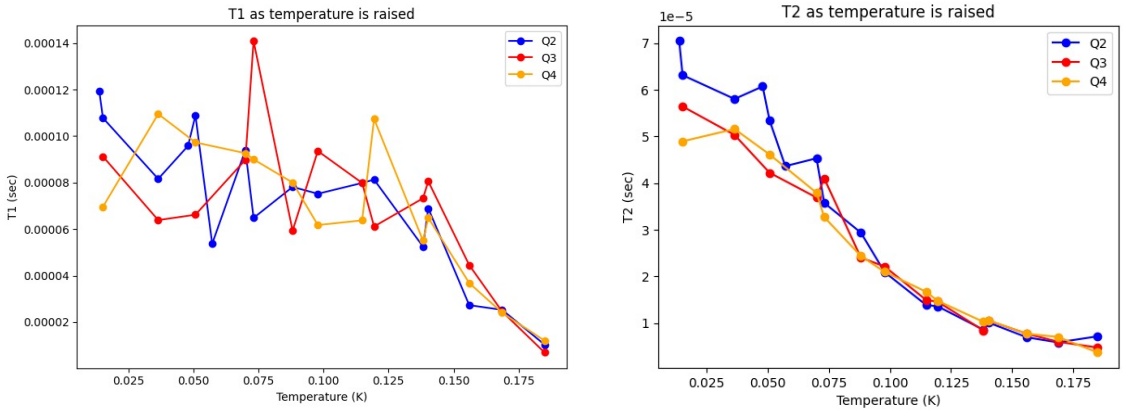

Figure 7: Temperature-dependent data of T_1 and T_2. (a) T_1 temperature dependence. At the lowest temperature, T_1 shows much variation for all three qubits. As temperature is raised, T_1 appears to maintain its length until around 120 mK before it beings decreasing. At this same threshold, the T_1 times for all three qubits begin to converge onto one value. (b). T_2 temperature dependence. Like T_1, T_2 begins with variation between at three qubits. As temperature is raised, T_2 begin diminishing around 30 mK and exhibits a similar converging behavior. T_2 appears to be more sensitive to temperature than T_1.

The T_2 data showed that transverse relaxation was almost immediately affected by temperature, showing a clear diminishing trend over every increased temperature interval. Second, a similar convergence of data points occurred which started at a much lower temperature than the T_1 data. T_2 is also known to fluctuate with time as shown in Figure 8, which is a reasonable source of noisy data, however, comparing the T_2 plot with T_1 suggests that T_2 is much more sensitive to increases in temperature.

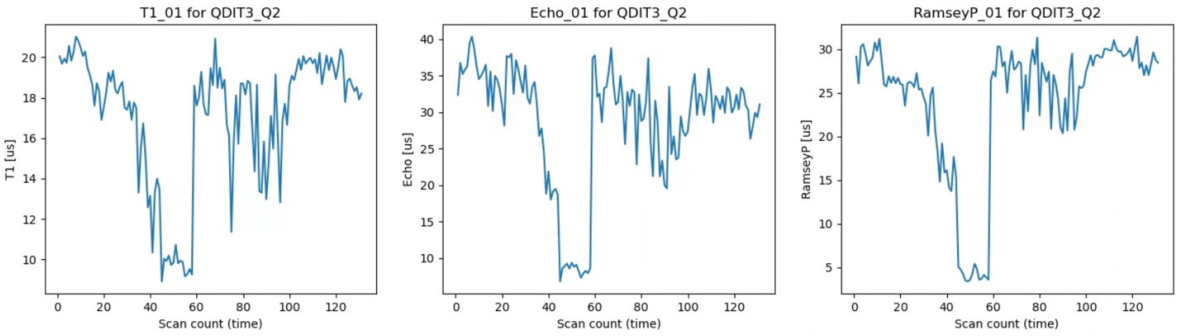

Figure 8: Decoherence fluctuations with time. (a) Extracted T_1 values from T_1 scan procedure plotted against time (or number of scans) show that there is large variation with a range of around 10 μs. (b) T_2 value from an Echo measurement plotted against time shows more variation with a range of around 30 μs. (c) Ramsey scan plotted against time shows variation with a range of around 25 μs.

Due to the relationship between T_1, T_2, and T_ϕ (eq. 1.3), knowing the T_2 and T_1 times allows us to solve for T_ϕ at each of the temperature data points. The T_ϕ data shows a very similar trend to the temperature dependence of T_2 as both the convergence and diminishing begin almost immediately with temperature and has less variation than T_1.

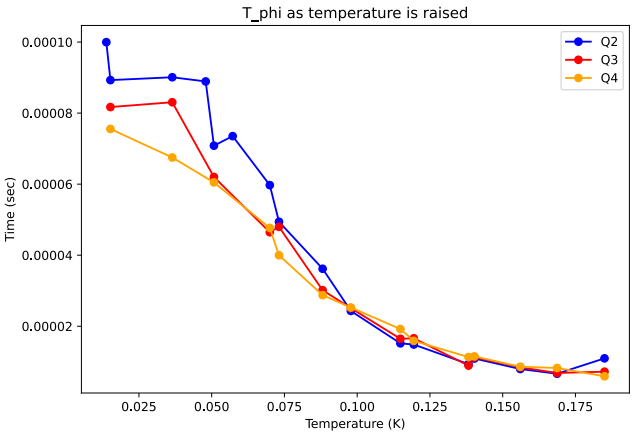

Figure 9: Temperature-dependent data of T_ϕ after a rearrangement. T_ϕ appears to maintain its value until a threshold of around 30 mK. The data shows a converging behavior like all other decoherence times at the same threshold temperature as T_2. T_ϕ resembles the T_2 data especially at the upper temperature points.

3.2 Model Fitting and Corresponding Theory

As discussed by Koch, et al. in their development of the transmon, the main mechanism for the dependence of T_1 with temperature is due to quasiparticles, which occur due to the thermal breaking of Cooper pairs [8]. These quasiparticles may be created by exciting a Cooper pair near the Josephson junction over the superconducting gap, , and their population is increased as the temperature is raised [16]. The number of conduction electrons can be calculated and thus the number of quasiparticles can be estimated. Moreover, the rate of quasiparticle tunneling across the junction can be calculated and based on these calculations, the longitudinal relaxation due to quasiparticle can be given as [8],

$$\Gamma_1 = 1/T_1 \simeq \Gamma_{qp} N_{qp} \sqrt{\frac{k_B T}{\hbar \omega_{01}}} \left| \langle g, n_g \pm 1/2 \mid e, n_g \rangle \right|^2 ,$$

where Γ_{qp} represents the rate of quasiparticle tunneling, N_{qp} represents the number of quasiparticles, k_B is Boltzmann's constant, $\hbar$ is reduced Planck's constant, $omega_q$ is the qubit's transition frequency, and the remaining expression represents a Modified Bessel function of the second kind. Notice the temperature parameter in the equation above. As a result, T_1 decreases as the temperature is raised due to the thermal activation of quasiparticles which damp the qubit mode [16]. The inverse quality factor ($Q = T_1 \omega_q$) of a junction due to quasiparticles can be modeled as [16],

$$\frac{1}{Q} = \frac{x_{ne}}{\pi} \sqrt{\frac{2\Delta}{\hbar\omega}} + \frac{2}{\pi} e^{-\frac{\Delta}{k_b T}} e^{-\frac{\hbar\omega}{2k_b T}} K_0 \left(\frac{\hbar\omega}{2k_b T} \right) \left[1 + e^{-\frac{\hbar\omega}{k_b T}} \right] ,$$

where $x_n e$ represents the population of non-equilibrium quasiparticles. Fitting the quasiparticle theory to T_1, we can see that the model does accurately fit our data and is consistent.

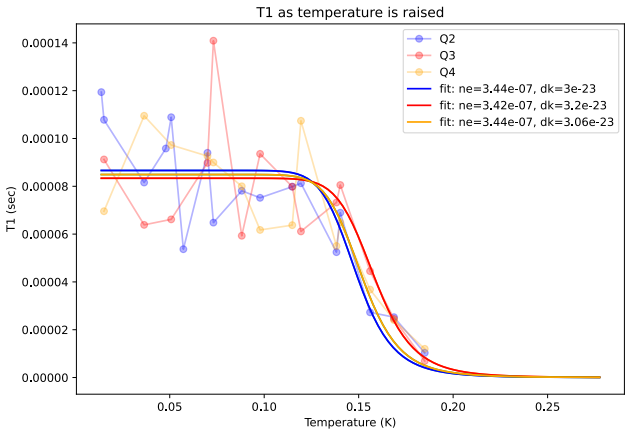

Figure 10: Quasiparticle model fit for T_1 data. A fit was done for each set of data points from each qubit (Q2, Q3, Q4).

The main mechanism for T_ϕ is believed to be photon-induced dephasing as discussed by Sears in his paper aiming to extend coherence times. Transmon readout resonators are designed to allow readout through a photon line. However, stray photons from the thermal population of the cavity that we cannot eliminate may cause dephasing. In the Hamiltonian [10],

$$H = \omega_r \widehat{N} + \frac{1}{2}\omega_q \hat{\sigma}_z + \frac{1}{2}\chi \widehat{N} \hat{\sigma}_z,$$

it is seen that the qubit frequency will shift by $\chi \sim 2g^2/\Delta$ for each photon in the resonator which will effectively dephase the qubit. These photons are induced by physically raising the temperature of the resonator. It can then be generalized for a qubit with an average number of photons in the resonator, $\bar{n} = 1/\left(\exp\left(\hbar\omega_c/k_T\right) - 1\right)$, will dephase at a rate [16]:

$$\gamma_\phi^{\text{tot}} = \frac{\kappa}{2}\Re\left[\sqrt{\left(1 + \frac{2i\chi}{\kappa}\right)^2 + \left(\frac{8i\chi}{\kappa}\right)} - 1\right].$$

It is assumed here that only one resonator is considered per qubit. $\Re$ represents taking the real portion of the bracketed expression. Because κ, a measure of how lossy a resonator is (also width of the resonator), and χ, the shift of the qubit frequency in response to the resonator, can be measured independently these become known constants for the fit. However, it was needed to introduce a constant as a fit parameter to match the model to our data. Furthermore, a curve fit with κ left variable did produce better fit results. This inaccuracy is believed to be due to the fact that the data was measured with an Echo scan rather than a Ramsey measurement, because an Echo is meant to reduce noise by being robust to the detuning frequency.

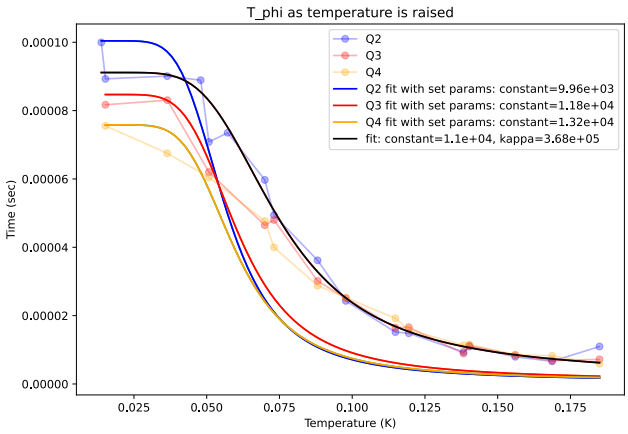

Figure 11: T_ϕ model fits based on photon-induced theory. All parameters of the fit were known, however, a constant was needed to be introduced as a parameter. Blue, red, and orange fits represent a curve fit for each of their respective qubits with only an arbitrary constant as a parameter. The error of the fits is believed to be due to using Echo measurements to extract T_2 rather than a Ramsey measurement. A fit with one parameter, κ, variable is shown for Q2 represented by the black line which shows superior fit.

For the T_2 model, I consider a combination by combining both temperature-dependent quasiparticle noise and photon-induced noise. Simply observing the three data plots, we see that at higher temperatures T_2 almost identically matches the T_ϕ data meaning photon-induced noise takes over in this regime. However, at the lower end of the temperature range, the T_2 data becomes much more random from both T_1 and T_ϕ. Given the nature of the relation of T_2 to T_1 and T_ϕ, it is known that T_2 may never at any time be greater than either T_1 or T_ϕ, and physically means at least one of these noises must limit T_2. The generalization of T_2 can be represented as,

$$\Gamma_2 = \frac{\Gamma_1}{2} + \Gamma_\phi$$

$$T_2 = \frac{1}{2T_1} + \frac{1}{T_\phi}$$

$$T_2 = \frac{1}{2\omega}\left(\frac{x_{ne}}{\pi}\sqrt{\frac{2\Delta}{\hbar\omega}} + \frac{2}{\pi}e^{-\frac{\Delta}{k_bT}}e^{-\frac{\hbar\omega}{2k_bT}}K_0\left(\frac{\hbar\omega}{2k_bT}\right)\left[1+e^{-\frac{\hbar\omega}{k_bT}}\right]\right)^{-1} + \left(\frac{\kappa}{2}R\left[\sqrt{\left(1+\frac{2i\chi}{\kappa}\right)^2 + \left(\frac{8i\chi\Sigma_j n_j K_j}{\kappa^2}\right)} - 1\right] + C\right)^{-1},$$

where the four parameters are x_{ne}, Δ, κ, C which represent non-equilibrium quasiparticle population, superconducting gap size, width of resonator, and a constant, respectively. Since all of these parameters of this equation can be known from the T_1 and T_ϕ model fits, plugging in these extracted values for the four fit parameters we see that this model quite accurately models the T_2 data. Furthermore, we compare the extracted fit parameters of a pure model fit with all four parameters as fit parameters which give us not the same values but the same order of magnitude.

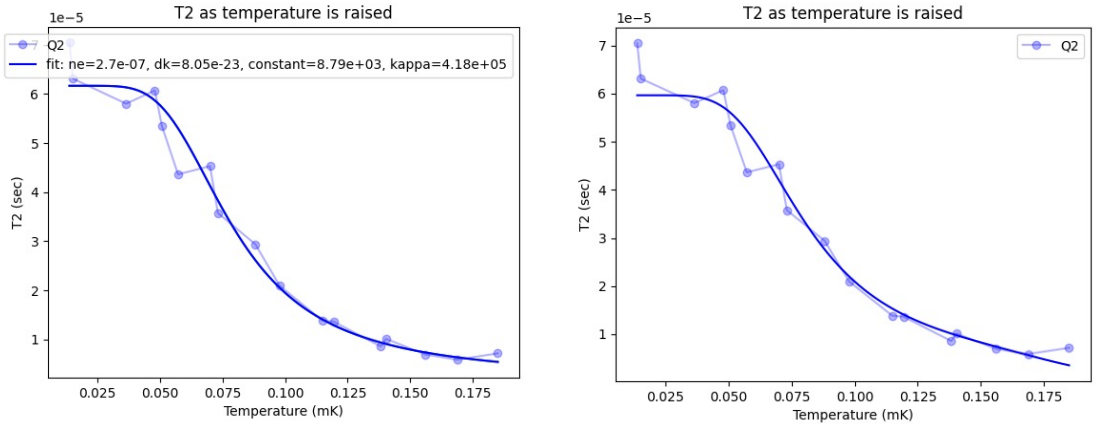

Figure 12: T_2 model fit based on a combined quasiparticle and photon-induced theory. (a) Model fit with all four fit parameters variable gives a superior fit. (b) Model fit with known parameters known from previous T_1 and T_ϕ fits. Error between the curve fit and known parameters is believed to be due to variation between an Echo scan instead of Ramsey measurement.

Lastly, in all three data plots, we see a clear convergence of qubit decoherence of all forms as the temperature increases. In T_1 this convergence becomes pronounced as the temperature begins to cross the threshold of around 120 mK. While noise at temperatures below this threshold is largely affected by the time fluctuations of T_1, above the threshold the quasiparticle tunneling noise will begin to overpower all other sources of noise (fluctuations induced over time) causing the convergence onto one line. The standard deviation of the T_1 times of the three measured qubits suddenly decreases. In both T_2 and T_ϕ we see the convergence almost immediately (∼30 mK) indicating the photon-induced noise is in effect at relatively low temperatures. Like the quasiparticle noise, the convergence suggests that photon-induced noise begins to overpower all other forms of noise or fluctuations to cause the convergence. While this convergence is only present at higher temperatures for all decoherence times and thus shortens decoherence times, it may be advantageous in certain scenarios to sacrifice decoherence times for more identical times.

I propose that temperature can be used to level the coherence performance of all qubits on a given chip allowing other metrics of qubit performance to be more meaningful. A major problem in currently improving qubit design is tied to identifying how and why one qubit is better than another [11]. With so many fluctuations in the performance of a qubit (even fluctuating with time), it makes it incredibly difficult to consistently evaluate its performance. Using this converging phenomenon, it is possible to level the decoherence times of all the qubits and perform other measurements. Notably, quantum logic gates are critical in controlling a qubit into a desired state for computation or measurement. Gate fidelity can be measured with state tomography, however, it is difficult to determine if the operation was inaccurate or if the qubit simply had a poor coherence. Making decoherence times identical may allow us to separate the effects of faulty gate calibration from decoherence effects.

3.3 Classical Analogy (RLC Circuit)

The classical RLC (resistor-inductor-capacitor) circuit acts as a harmonic oscillator like the LC by storing energy that oscillates at the circuit's resonant frequency. However, the RLC incorporates a resistor that directly affects damping, the decay of oscillations over time. An important metric to characterize damping and resonators is the Quality (Q) factor. It is defined as the ratio between the initial amount of energy stored in the circuit to the lost energy after one cycle of oscillation [1]. Mathematically, this assumes the form

$$Q = \frac{\omega_o}{\Delta\omega}.$$

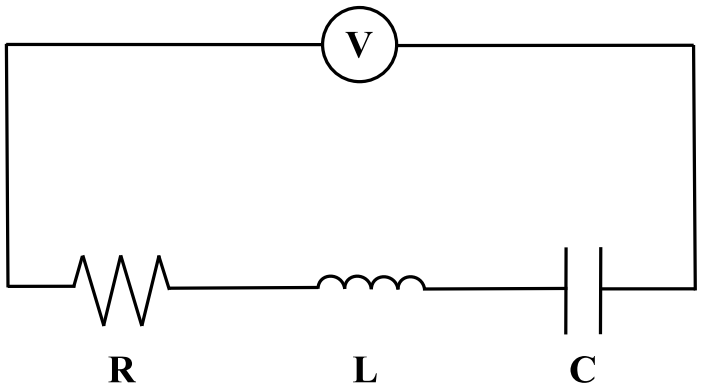

Figure 13: Classical RLC (resistor-inductor-capacitor) circuit in series. V represents a power source, R represents the resistor, L is the inductor, and C is the capacitor. An RLC circuit acts as a harmonic oscillator that is damped by the introduction of a resistor.

A system that loses much energy to damping will have a low-Q, whereas high-Q circuits are under-damped. The Q factor of an RLC circuit can be calculated as,

$$Q = \frac{1}{R}\sqrt{\frac{L}{C}},$$

where L is inductance and C is capacitance. Notice especially the inverse relationship resistance has with the quality factor. Now, because a transmon acts very similar to an LC circuit, just quantized, using the same definition for quality factor it is possible to get the order of magnitude relation [13],

$$Q \approx T_1 \omega_q.$$

Because the Q factor (and thus T_1) decreases as the temperature is raised due to the thermal activation of quasiparticles which damp the qubit mode [16], this relationship with temperature can be modeled with the classical RLC circuit.

Imagining a thermistor whose resistance increases as temperature increases, then the quality factor of the RLC circuit must then decrease if the temperature is raised. Physically, this is because as current oscillates within the RLC circuit, the resistor will cause some of this energy to be converted to heat and be lost into the environment. Similarly, if the population of quasiparticles increases as a function of temperature, this will cause the qubit to lose more energy to its environment. It can then be said that the number of quasiparticles in a system can be compared to the resistor of the RLC circuit analogously as the mechanism that causes loss in T_1 as temperature is raised. Furthermore, the entire transmon qubit can be analogously compared to the RLC circuit as a whole since it acts like a harmonic oscillator. It is easy to physically make an RLC circuit to explain the transmon. This analogy is important to demonstrate on a human scale not only how a qubit operates but also how decoherence works, especially as the temperature is raised. Because while the quantum world is invisible and differs strongly from our classically defined world, many of its processes can be thought or built analogously that can help us visualize and understand them better and give us new perspective.

4 Discussion

4.1 Impact

Understanding the temperature dependence of qubit decoherence in both an analytical and physical way allows us to understand the fundamental noise sources that limit the qubit from achieving longer decoherence times. T_1 is limited by quasiparticles while T_ϕ is limited by photon noise in the readout resonators. The T_2 model provides insight into the noise that limits T_2 as temperature is raised in

both the form of a physical mechanism – quasiparticles and thermally-induced photons – and also a mathematical model that describes its dependence. Importantly, to push for overall better qubits and quantum computers that can operate in higher temperatures, new qubit designs may be focused to eliminate these two sources of noise that suppress decoherence times.

Furthermore, observation of the convergence of decoherence times as temperature is raised shows how sources of noise begin to overpower other sources of noise like time-dependent fluctuations of decoherence. In addition, based on this convergence phenomenon, a thermally induced decoherence-identical chip may allow all qubits on that chip to be leveled to the same coherence performance allowing other performance metric measurements to be more meaningful. Because of the many fluctuations present that affect qubit performance, it is extremely challenging to discern if and how one qubit may be better than another. Without the ability to identify how and why one slightly different qubit is better than another, making incremental improvements and progress to optimize qubit circuits are incredibly difficult and are forced to try make drastic changes that are rare and even harder to achieve [11]. Using temperature to dramatically limit the variation of all decoherence times thus becomes important in identifying how and why a qubit may be better than another and allows us to improve our qubits in a much more productive way.

4.2 Future Work

I proposed that a thermally-induced decoherence-identical qubit chip is beneficial in scenarios to isolate metrics of qubit performance like gate fidelity. Future work may focus on other scenarios where a decoherence-identical chip may be beneficial and applying this method. Furthermore, future work may focus on designing these qubits to have a "sweet spot" temperature where the thermal population does not interfere much with the accuracy of measurements while also gaining a decoherence-identical property.

Another avenue involves thermodynamics. When increasing the fridge temperature with the resistor, it was noticed that the relationship between temperature and power was non-linear. This could be due to the fridge's thermal conductivity or the cooling power of the fridge also being temperature dependent. If the cooling power increases as the temperature is raised, such a trend between temperature and power passed through the resistor, as shown in Figure 14, would be possible. Further research can be conducted to investigate the thermodynamic physical mechanism for a non-linear relationship and develop a model to predict the fridge temperature as a function of resistor power.

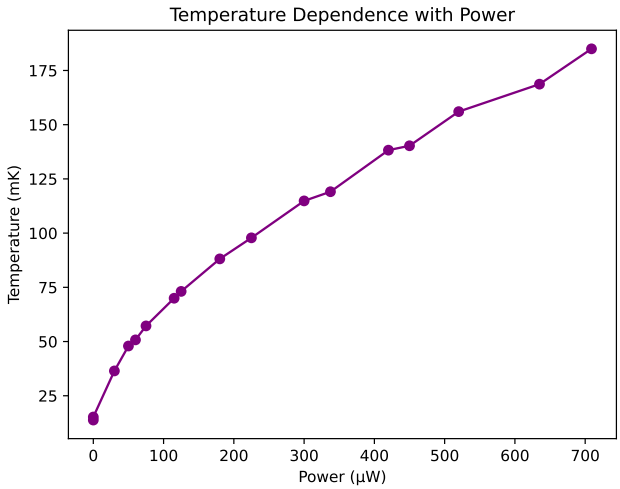

Figure 14: Plot of fridge temperature as a function of resistor power. It is clear that temperature increases in a non-linear relationship which was not expected.

5 Conclusion

While superconducting qubits are extremely promising in their application for quantum computing because of their fast gate times and reproducibility [5], an outstanding challenge remains in achieving long enough decoherence times to perform useful computations. At higher environment temperatures the decoherence of qubits decreases. Understanding this fundamental temperature limit provides insight into the overall limits of qubit coherence.

This research work investigates models for the temperature dependence of T_1 and T_ϕ based on quasiparticle noise and photon-induced noise, respectively. Based on these findings, a model for T_2 is explored considering both quasiparticle and photon noise and in which regimes each applies. Additionally, this research explains the convergence of decoherence times for multiple qubits on one chip as the temperature is raised. I then propose an optimization by thermally inducing a decoherence-identical chip to level the decoherence performance of all qubits on a chip to better evaluate gate fidelity. Finally, a classical analogy to the RLC circuit was outlined to better demonstrate the relationship between qubit decoherence and temperature. Analyzing all of these results allows for a better understanding of the dependence of decoherence with temperature, an important aspect of quantum computer operation at higher temperatures.

6 Acknowledgements

I would like to firstly thank Prof. Machiel Blok for his guidance and for providing me the opportunity to conduct research in his lab this summer. Next, I owe my greatest gratitude to my mentor, Ray Parker, for his continued support and invaluable suggestions and also Zihao Wang for useful discussions. In addition, thank you to Ana Fontan for helping collect some of the data together with me. This research was conducted as part of the University of Rochester Research Experience for High Schoolers (REH) program sponsored by the Center for Matter at Atomic Pressures.

References

[1] Agarwal, A. and Lang, J. (2005). *Foundations of analog and digital electronic circuits*. Elsevier.

[2] Arute, F., Arya, K., Babbush, R., Bacon, D., Bardin, J. C., Barends, R., Biswas, R., Boixo, S., Brandao, F. G., Buell, D. A., et al. (2019). Quantum supremacy using a programmable superconducting processor. *Nature*, 574(7779):505–510.

[3] Caldwell, S., Didier, N., Ryan, C., Sete, E., Hudson, A., Karalekas, P., Manenti, R., da Silva, M., Sinclair, R., Acala, E., et al. (2018). Parametrically activated entangling gates using transmon qubits. *Physical Review Applied*, 10(3):034050.

[4] Castelvecchi, D. (2017). Quantum computers ready to leap out of the lab in 2017. *Nature*, 541(7635).

[5] Clarke, J. and Wilhelm, F. K. (2008). Superconducting quantum bits. *Nature*, 453(7198):1031–1042.

[6] Davies, P. (1978). The tailor-made universe. *Sciences*, 18:6–10.

[7] Gambetta, J. M., Chow, J. M., and Steffen, M. (2017). Building logical qubits in a superconducting quantum computing system. *npj quantum information*, 3(1):1–7.

[8] Koch, J., Terri, M. Y., Gambetta, J., Houck, A. A., Schuster, D. I., Majer, J., Blais, A., Devoret, M. H., Girvin, S. M., and Schoelkopf, R. J. (2007). Charge-insensitive qubit design derived from the cooper pair box. *Physical Review A*, 76(4):042319.

[9] Konik, R. (2021). Quantum coherence confined. *Nature Physics*, 17(6):669–670.

[10] Krantz, P., Kjaergaard, M., Yan, F., Orlando, T. P., Gustavsson, S., and Oliver, W. D. (2019). A quantum engineer's guide to superconducting qubits. *Applied Physics Reviews*, 6(2):021318.

[11] McRae, C. R. (2018). Indium thin films in multilayer superconducting quantum circuits.

[12] Nakamura, Y., Pashkin, Y. A., and Tsai, J. (1999). Coherent control of macroscopic quantum states in a single-cooper-pair box. *nature*, 398(6730):786–788.

[13] Nielsen, M. A. and Chuang, I. (2002). Quantum computation and quantum information.

[14] O'Malley, P. J. J. (2016). *Superconducting qubits: dephasing and quantum chemistry*. University of California, Santa Barbara.

[15] Roth, T. E., Ma, R., and Chew, W. C. (2021). An introduction to the transmon qubit for electromagnetic engineers. *arXiv preprint arXiv:2106.11352*.

[16] Sears, A. P. (2013). *Extending Coherence in Superconducting Qubits: from microseconds to milliseconds*. Yale University.

[17] Verjauw, J., Acharya, R., Van Damme, J., Ivanov, T., Lozano, D. P., Mohiyaddin, F., Wan, D., Jussot, J., Vadiraj, A., Mongillo, M., et al. (2022). Path toward manufacturable superconducting qubits with relaxation times exceeding 0.1 ms. *arXiv preprint arXiv:2202.10303*.

[18] Vu, C. (2016). Ibm makes quantum computing available on ibm cloud to accelerate innovation. *IBM News Room*.

[19] Youssef, R. (2020). Measuring and simulating t1 and t2 for qubits. Technical report, Fermi National Accelerator Lab.(FNAL), Batavia, IL (United States).